Article:
Cornel, E.J., Smith, G.N., Rogers, S.E. et al. (2020) Time-resolved small-angle neutron scattering studies of the thermally-induced exchange of copolymer chains between spherical diblock copolymer nanoparticles prepared via polymerization-induced self-assembly. Soft Matter, 16 (15). pp. 3657-3668. ISSN: 1744-683X

https://doi.org/10.1039/c9sm02425e

ARTICLE

Time-resolved small-angle neutron scattering studies of the thermally-induced exchange of copolymer chains between spherical diblock copolymer nanoparticles prepared via polymerization-induced self-assembly

Received 00th January 20xx,
Accepted 00th January 20xx

DOI: 10.1039/x0xx00000x

Erik J. Cornel,[a] Gregory N. Smith,[a,b] Sarah E. Rogers,[c] James E. Hallett,[d] David J. Growney,[e] Timothy Smith,[e] Paul S. O'Hora,[e] Sandra van Meurs,[a] Oleksandr O. Mykhaylyk[a,†] and Steven P. Armes[a,†]

Sterically-stabilized diblock copolymer nanoparticles (a.k.a. micelles) are prepared directly in non-polar media via polymerization-induced self-assembly (PISA). More specifically, a poly(lauryl methacrylate) chain transfer agent is chain-extended via reversible addition-fragmentation chain transfer (RAFT) dispersion polymerization of methyl methacrylate (MMA) to form sterically-stabilized spheres at 20% w/w solids in *n*-dodecane at 90 °C. Both fully hydrogenous ($PLMA_{39}$-$PMMA_{55}$ and $PLMA_{39}$-$PMMA_{94}$) and core-deuterated ($PLMA_{39}$-d_8PMMA_{57} and $PLMA_{39}$-d_8PMMA_{96}) spherical nanoparticles with mean core diameters of approximately 20 nm were prepared using this protocol. After diluting each dispersion in turn to 1.0% w/w with *n*-dodecane, small-angle X-ray scattering studies confirmed essentially no change in spherical nanoparticle diameter after thermal annealing at 150 °C. Time-resolved small angle neutron scattering was used to examine whether copolymer chain exchange occurs between such nanoparticles at elevated temperatures. Copolymer chain exchange for a binary mixture of $PLMA_{39}$-$PMMA_{55}$ and $PLMA_{39}$-d_8PMMA_{57} nanoparticles produced hybrid (mixed) cores containing both $PMMA_{55}$ and d_8PMMA_{57} blocks within 3 min at 150 °C. In contrast, a binary mixture of $PLMA_{39}$-$PMMA_{94}$ and $PLMA_{39}$-d_8PMMA_{96} nanoparticles required 8 min at this temperature before no further reduction in neutron scattering intensity could be observed. These observations suggest that the rate of copolymer chain exchange depends on the degree of polymerization of the core-forming block. Relatively slow copolymer chain exchange was also observed at 80 °C, which is below the T_g of the core-forming PMMA block as determined by DSC studies. These observations confirm rapid exchange of individual copolymer chains between sterically-stabilized nanoparticles at elevated temperature. The implications of these findings are briefly discussed in the context of PISA, which is widely recognized as a powerful route to a range of sterically-stabilized nanoparticles.

Introduction

Traditionally, well-defined diblock copolymers are prepared via anionic polymerization using a good solvent for both blocks.[1,2] Subsequently, micellar self-assembly can be achieved using a solvent switch, with this post-polymerization processing step typically being conducted in dilute solution.[3–5] However, anionic polymerization requires rigorously anhydrous conditions and is restricted to a relatively narrow range of vinyl (or cyclic) monomers. In contrast, reversible addition-fragmentation chain transfer (RAFT) polymerization[6–12] involves radical chemistry and hence enables the synthesis of a wide range of near-monodisperse *functional* diblock copolymers using much less demanding reaction conditions (i.e. monomer and solvent purification is not required).[13–20] Moreover, RAFT polymerization is well-suited for polymerization-induced self-assembly (PISA).[21–27] This technique involves chain extension of a soluble homopolymer precursor using a second monomer that grows to form an insoluble block on reaching a certain critical degree of polymerization (DP). This drives *in situ* self-assembly, leading to the formation of sterically-stabilized diblock copolymer nanoparticles. Notably, PISA enables the convenient and highly efficient preparation of various types of diblock copolymer nanoparticles directly at high solids (up to 50% w/w).[28] RAFT-mediated PISA syntheses can be performed in many solvents, with both aqueous and alcoholic formulations being widely reported in the literature.[24,29,30] However, there

[a] *Dainton Building, Department of Chemistry, University of Sheffield, Brook Hill, Sheffield, South Yorkshire S3 7HF, UK.*
[b] *Niels Bohr Institute, University of Copenhagen, Universitetsparken 5, 2100 Copenhagen Ø, Denmark.*
[c] *Rutherford Appleton Laboratory, Harwell Oxford, Didcot OX11 0QX, UK.*
[d] *H.H. Wills Physics Laboratory, University of Bristol, Tyndall Avenue, Bristol BS8 1TL, UK.*
[e] *Lubrizol Ltd, Nether Lane, Hazelwood, Derbyshire, DE56 4AN, UK.*
† Authors to whom correspondence should be addressed (s.p.armes@sheffield.ac.uk and o.mykhaylyk@sheffield.ac.uk).
Electronic Supplementary Information (ESI) available: [NMR analysis of crude PLMA precursor block, crude PLMA-PMMA and PLMA-d_8PMMA, SAS models for dissolved polymer chains and diblock copolymer nanoparticles Variable temperature proton NMR for dilute dispersions of PLMA-PMMA spheres, variable temperature SANS on PLMA-d_8PMMA spheres, R(t) analysis of TR-SANS data, DSC measurements on PMMA homopolymers.]. See DOI: 10.1039/x0xx00000x

are rather fewer reports of syntheses in non-polar media, yet they offer considerable potential.[21,25,28,31–34]

In principle, the RAFT-mediated PISA of methacrylic monomers enables the rational synthesis of diblock copolymer spheres, worms or vesicles by careful selection of the target block composition and copolymer concentration.[33] Although kinetically-trapped spheres are commonly observed, it is well-known that spheres can evolve to form highly anisotropic worms during PISA under certain conditions.[13,35–38] Moreover, worm formation is generally favored at higher copolymer concentration, which suggests that the sphere-to-worm transition is likely to proceed via the 1D fusion of multiple spheres.[28,33,35] There is good precedent for copolymer chain exchange between diblock copolymer micelles (i.e. sterically-stabilized nanoparticles) in both aqueous and non-aqueous media.[39,40,49–54,41–48] Two principal mechanisms have been suggested for this process in the literature: (i) the chain expulsion/insertion mechanism and (ii) the micelle fusion/fission mechanism.[40,55–59] It appears to be generally accepted that the latter mechanism is energetically demanding, and hence most likely not applicable for diblock copolymer micelles under normal experimental conditions.[44] Moreover, dynamic light scattering and proton NMR studies provide direct evidence for a population of molecularly-dissolved copolymer chains on heating polystyrene-core micelles in *n*-heptane to 90 °C, which is consistent with the expulsion/insertion mechanism.[60] However, as discussed earlier, fusion/fission is the most likely explanation for the formation of highly anisotropic worms during PISA. Therefore it seems likely that both mechanisms are important during such syntheses. Furthermore, in the context of PISA, it is interesting to consider whether copolymer chain exchange occurs between monomer-swollen diblock copolymer nano-objects either during the growth of kinetically-trapped spheres[21,25] and/or during the evolution in copolymer morphology from spheres to worms to vesicles.[22,25,28,33,35]

Both Willner, Lund and co-workers,[39,43,47,50–54] and the Minnesota group led by Bates and Lodge[5,40–42,44–46,48,61] have examined the rate and extent of copolymer chain exchange between diblock copolymer micelles using the contrast variation approach to conduct time-resolved small-angle neutron scattering (TR-SANS) experiments. However, the latter team's work is more relevant to the present study, because they consider copolymer exchange between micelles in non-polar media. For example, Choi and co-workers studied mixtures of hydrogenous and partially deuterated poly(ethylene-alt-propylene)-polystyrene (PEP-PS) spherical diblock copolymer nanoparticles. These nanoparticles were dispersed in a binary mixture of hydrogenous and deuterated squalane to produce 1.0% v/v dispersions of polystyrene-core micelles.[40] These two dispersions were then combined in a 1:1 ratio by volume and analyzed by TR-SANS. A distinct scattering pattern was obtained for the initial dispersion, since this comprised a binary mixture of two distinct types of micelles containing either deuterated or hydrogenous polystyrene cores, with the binary solvent composition being chosen to produce a neutron scattering length density (SLD) lying halfway between that of the two types of micelle cores. However, a gradual reduction in neutron scattering intensity was observed on heating to 100–145 °C, suggesting copolymer chain exchange between the initial micelles driven by entropic mixing.[40] The extent (and rate) of chain mixing increased significantly at higher temperatures and the exchange kinetics could be fitted using a 'single chain exchange' model. Moreover, using longer core-forming polystyrene blocks led to a much slower rate of copolymer chain exchange.[40] Subsequent studies by the Minnesota team examined the effect of (i) higher copolymer concentrations,[41] (ii) varying the molecular weight distribution,[42] (iii) the behavior of binary mixtures of diblock copolymers with differing core-forming block DPs,[44] (iv) copolymer architecture (i.e. diblocks vs. triblocks),[45] and (v) addition of corona block in the form of free homopolymer.[46]

Herein we explore whether copolymer chain exchange occurs between hydrogenous poly(lauryl methacrylate)$_{39}$-poly(methyl methacrylate)$_x$ [PLMA$_{39}$-PMMA$_x$] and the analogous core-deuterated [PLMA$_{39}$-d$_8$PMMA$_x$] spherical nanoparticles prepared directly in *n*-dodecane via RAFT PISA. First, the spherical nanoparticles were characterized by small-angle X-ray scattering (SAXS). Subsequently, TR-SANS was used to assess whether copolymer chain exchange occurs for this particular diblock copolymer system when varying (i) temperature and (ii) the DP of the core-forming PMMA block. Understanding the behavior of such sterically-stabilized nanoparticles at elevated temperature is expected to provide useful insights regarding the evolution in copolymer morphology during PISA.

Experimental

Materials. Lauryl methacrylate and methyl methacrylate were purchased from Sigma-Aldrich (UK) and deuterated methyl methacrylate was purchased from Apollo Scientific (UK). Each monomer was passed through basic alumina to remove its inhibitor prior to use. Tert-Butylperoxy-2-ethylhexanoate (Trigonox 21S or T21s) initiator was supplied by AkzoNobel (The Netherlands). THF, *n*-dodecane, triethylamine, butylated hydroxytoluene, 2-propanol and 2,2-azobis(2-methylpropionitrile) (AIBN) were purchased from Sigma-Aldrich (UK) and used as received. 4-Cyano-4-((2-phenylethanesulfonyl)thiocarbonylsulfanyl)pentanoic acid (PETTC) was prepared in-house according to a well-established protocol.[62] Both d$_{26}$-dodecane (C$_{12}$D$_{26}$) and d$_2$-dichloromethane (CD$_2$Cl$_2$) were obtained from Cambridge Isotope Laboratory (Tewksbury, USA) while d-chloroform (CDCl$_3$) was purchased from VWR (Lutterworth, UK).

Synthetic Protocols

Synthesis of PLMA precursor via RAFT solution polymerization of LMA. A PLMA$_{39}$ precursor (macro-CTA) was prepared via RAFT solution polymerization of LMA (59.95 g, 235.6 mmol) at 70 °C in toluene (62 g) using PETTC (2.00 g, 5.89 mmol; target DP = 40) and AIBN initiator (0.19 g, 1.18 mmol; PETTC/AIBN molar ratio = 5.0) (**Scheme 1**). This polymerization was quenched after 4 h (76% conversion, see **Figure S1** and **Equation S1** in the Supporting Information) to avoid any loss of RAFT chain-ends under monomer-starved conditions. PLMA

was purified by precipitation into a ten-fold excess of methanol (three times) and dried under vacuum. A mean DP of 39 was determined via end-group analysis using proton NMR spectroscopy (CD_2Cl_2) by comparing the integrated aromatic PETTC signals at 7.18-7.38 ppm to those of the oxymethylene signals at 3.92–4.08 ppm assigned to the LMA repeat units (**Equation S2**). THF size exclusion chromatography (SEC) indicated a M_n of 9 700 and an M_w/M_n of 1.12 (**Figure 1**), which is consistent with previous studies of well-controlled RAFT polymerizations.

Synthesis of hydrogenous $PLMA_{39}$-$PMMA_x$ and core-deuterated $PLMA_{39}$-d_8PMMA_x diblock copolymer spheres via RAFT dispersion polymerization. Methyl methacrylate (MMA; 0.19 g, 1.89 mmol) was used for chain extension of a $PLMA_{39}$ macro-CTA (0.30 g, 0.029 mmol; target DP = 60) in 1.96 g *n*-dodecane at 20% w/w solids, using a T21s initiator (23 µl of a 10% v/v solution, targeting a macro-CTA/initiator molar ratio of 3.0) (**Scheme 1**). This reaction mixture was heated to 90 °C for 16 h. A final MMA conversion of 92% was determined by proton NMR analysis of the crude reaction mixture diluted in $CDCl_3$ (the integrated monomer vinyl signals at 5.59 and 6.13 ppm were compared to the integrated pendent methoxy signal assigned to the MMA repeat units at 3.6 ppm) (**Figure S2** and **Equation S3**). A PMMA DP of 100 was also targeted when using 0.31 g MMA (3.16 mmol) and 2.46 g *n*-dodecane and in this case the final MMA conversion was 94%. Core-deuterated nanoparticles were prepared via the same protocol by using d_8MMA instead of MMA. The densities for MMA, d_8MMA, PMMA and d_8PMMA are 0.936 g cm^{-3}, 1.011 g cm^{-3}, 1.188 g cm^{-3} and 1.255 g cm^{-3}, respectively.[63,64] Thus the difference between the monomer and polymer densities are 0.24 g cm^{-3} and 0.25 g cm^{-3} for the hydrogenous and deuterated blocks, which indicates almost identical volume contractions during the respective homopolymerizations of MMA and d_8MMA. Hence identical MMA and d_8MMA monomer volumes were used for these syntheses, which ensured comparable core volumes. However, small differences in the final monomer conversions led to minor differences in the block volumes of the hydrogenous and deuterated core-forming PMMA chains used for small-angle scattering (SAS) models (**Table S1**). Final d_8MMA conversions of 95% and 96% were determined by analyzing the crude reaction mixture using deuterium NMR spectroscopy (**Figure S3**); this approach indicated core-forming block DPs of 57 and 96, respectively (as calculated using **Equation S3**). These values are close to those calculated for the corresponding hydrogenous PMMA blocks.

Copolymer Characterization

SEC analysis. Molecular weight distributions were assessed by size exclusion chromatography (SEC) using THF as an eluent. The SEC set-up comprised an Agilent 1260 Infinity series degasser and pump, two Agilent PLgel 5 µm Mixed-C columns in series and a refractive index detector. The mobile phase contained 2.0% v/v triethylamine and 0.05% w/w butylhydroxytoluene (BHT) and the flow rate was fixed at 1.0 ml min^{-1}. Samples were dissolved in THF containing 0.50% v/v toluene as a flow rate marker prior to SEC analysis. A series of ten poly(methyl methacrylate) standards (M_p values ranging from 1 280 to 330 000 g mol^{-1}) were used for calibration.

NMR spectroscopy. Proton and deuterium NMR spectra were recorded in either $CDCl_3$, $CHCl_3$ or CD_2Cl_2 using a Bruker AVANCE III HD 400 or 500 MHz spectrometer. Spectra were analyzed using TopSpin version 3.1 software. For deuterium NMR studies, the spectrometer was locked using an NMR tube containing $CDCl_3$ prior to analysis, which was then removed and replaced with an NMR tube containing a solution of $PLMA_{39}$-d_8PMMA_x dissolved in $CHCl_3$. Deuterium NMR spectra were obtained at 76.77 MHz using an unlocked spectrometer to record 128 scans at 8 000 data points per spectrum over an acquisition window of 1.5 kHz and using a relaxation delay time of 5 seconds. Copolymer dispersions were dissolved using $CHCl_3$, the $CDCl_3$ signal was set to 7.26 ppm, and the integrated d_8MMA vinyl signals at 5.59 and 6.14 ppm were compared to those assigned to the integrated methoxy signals of d_8MMA monomer and d_8PMMA polymer between 4.25 ppm and 2.79 ppm.

Variable temperature proton NMR spectra were recorded at 400 MHz, using either a Bruker AVANCE III or a Bruker AVANCE III HD spectrometer. $PLMA_{39}$-$PMMA_{55}$ and $PLMA_{39}$-$PMMA_{94}$ spherical nanoparticles were diluted to 1.0% w/w in *n*-dodecane prior to analysis. Measurements were performed using d_8-DMSO as a lock solvent in an external capillary tube. Spectra were recorded at 20, 40, 80, 100, 120, 140 and 150 °C.

Small-angle X-ray scattering (SAXS). Measurements were performed using a Bruker Nanostar SAXS instrument modified with a GeniX3D microfocus Cu Kα X-ray tube and motorized scatterless slits for the beam collimation (Xenocs, France) and a 2D HiSTAR multiwire gas detector (Siemens/Bruker). Data were recorded over a q range of 0.009 Å^{-1} < q < 0.17 Å^{-1} using a sample-to-detector distance of 1.46 m, where q is defined as:

$$q = \frac{4\pi \sin\theta}{\lambda} \quad (1)$$

where 2θ is the scattering angle and λ is the incident radiation wavelength. Data were collected using 2 mm diameter glass capillaries (WJM-Glass Muller GMBH, Germany). Water, *n*-dodecane and a glassy carbon standard were used for absolute intensity calibration.[65] SAXS measurements were conducted on 1.0% w/w dispersions of either $PLMA_{39}$-$PMMA_x$ or $PLMA_{39}$-d_8PMMA_x nanoparticles in *n*-dodecane. Exposure times were 1800 s for the empty capillary and solvent background. Scattering data for the dilute copolymer dispersions (1.0% w/w) were collected for 500 s, whereas data for 1.0% w/w $PLMA_{39}$ homopolymer solutions were collected for 1800 s. SAXS patterns were fitted using either the Debye function[66] (**Equation S5**) or a spherical micelle model[67–69] (**Equations S6-S14** in the Supporting Information) after background subtraction using the Irena macros[70] for Igor Pro software.

Small-angle neutron scattering (SANS). TR-SANS studies were conducted using the SANS2d instrument at the ISIS Neutron Spallation Source (STFC Rutherford Appleton Laboratory, Didcot, UK). This time-of-flight (ToF) instrument was set up to

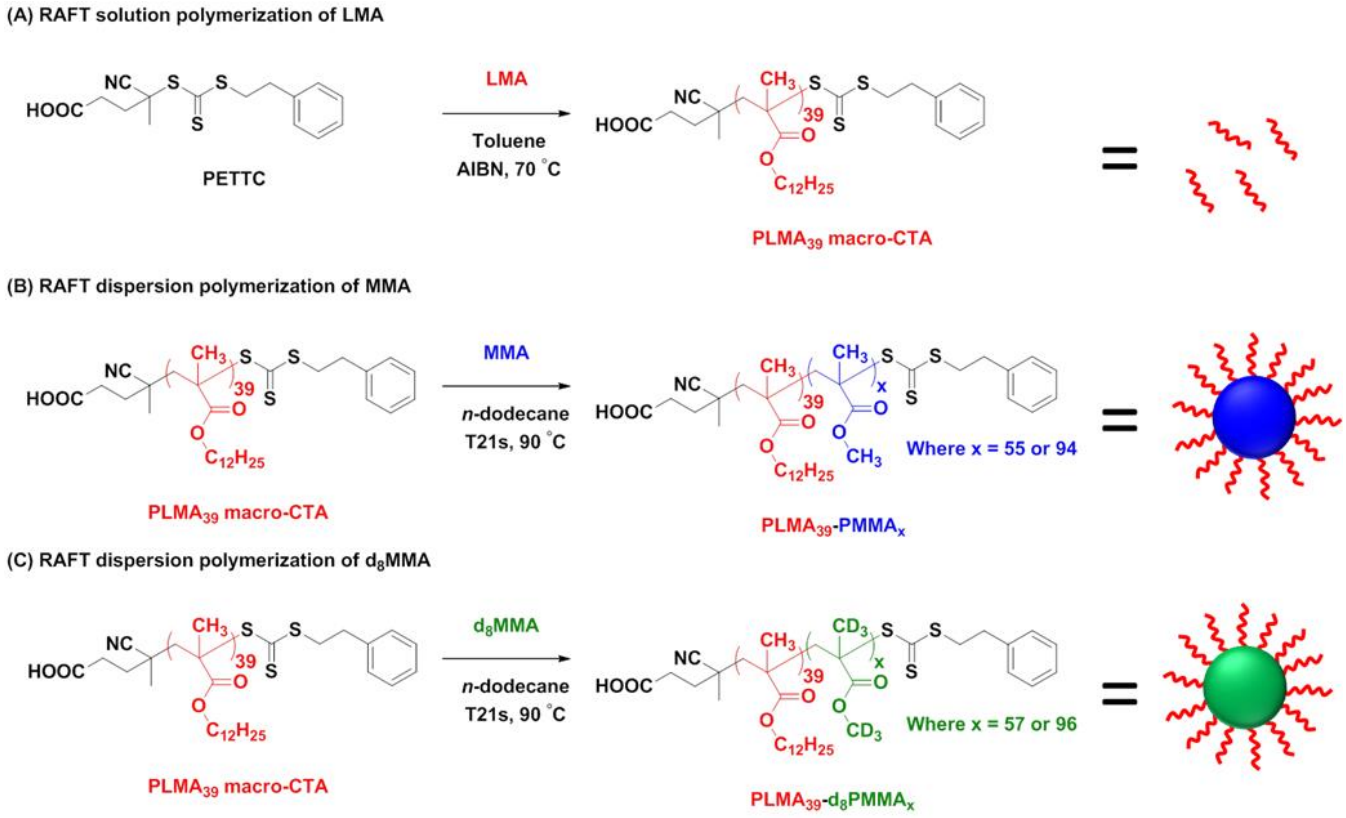

Scheme 1. (A) $PLMA_{39}$ homopolymer was prepared via RAFT solution polymerization of LMA in toluene at 70 °C. Subsequently, this precursor block was chain-extended with either (B) MMA or (C) d_8MMA in *n*-dodecane at 90 °C. This RAFT dispersion polymerization protocol was used to prepare the following four types of sterically-stabilized spherical nanoparticles: $PLMA_{39}$-$PMMA_{55}$, $PLMA_{39}$-d_8PMMA_{57}, $PLMA_{39}$-$PMMA_{94}$ and $PLMA_{39}$-d_8PMMA_{96}

Table 1. Summary of the characterization data obtained for the four types of diblock copolymer nanoparticles used in this study.

Composition[a]	M_n[b]	M_w/M_n[b]	Initial core diameter / nm[c]	Annealed core diameter / nm[c]	PMMA or d_8PMMA T_g / °C[d]
$PLMA_{39}$-$PMMA_{55}$	15 300	1.13	10.8 (± 1.2)	10.8 (± 1.2)	88.3
$PLMA_{39}$-d_8PMMA_{57}	16 000	1.13	11.2 (± 1.0)	11.2 (± 1.2)	81.9
$PLMA_{39}$-$PMMA_{94}$	18 600	1.14	14.6 (± 1.4)	14.6 (± 1.4)	87.9
$PLMA_{39}$-d_8PMMA_{96}	19 300	1.13	14.0 (± 1.2)	14.2 (± 1.2)	82.9

[a] The subscript denotes the mean degree of polymerization as determined by proton or deuterium NMR spectroscopy, respectively. [b] M_n and M_w/M_n values determined by THF SEC. [c] Nanoparticle core diameters with their corresponding standard deviations (in brackets) obtained from SAXS analysis before and after thermal annealing. [d] T_g values obtained from DSC analysis of purified diblock copolymers.

cover a scattering vector length, *q*, in the 0.0045 – 0.7 $Å^{-1}$ range. The wavelength range used for the ToF SANS experiments was 1.75 – 16.5 Å. The neutron beam diameter was 8 mm. Each raw scattering data set was corrected for the detector efficiency, sample transmission and background scattering and then converted into differential scattering cross-section per unit sample volume data ($\partial\Sigma/\partial\Omega$ vs. *q*) using instrument-specific software (Mantid). These data were placed on an absolute scale (cm^{-1}) using the scattering from a standard sample (a solid blend of hydrogenous and perdeuterated polystyrene) in accordance with established protocols. Raw data were sliced into 1-minute time frames using instrument-specific software; this provided sufficient resolution for further analysis.

Static SANS measurements were performed on the LOQ small-angle diffractometer at the ISIS Pulsed Neutron Source (STFC Rutherford Appleton Laboratory, Didcot, U.K.). A scattering pattern was recorded for 30 min over a *q* range of 0.008-0.254 $Å^{-1}$, using a sample-detector distance of 4 m. A 12 mm diameter beam was used with a neutron wavelength between 0.02 and 0.1 Å. Raw data were integrated, normalized with respect to transmission and intensity, and merged together using instrument-specific software, LAMP. Data were analyzed using the Irena package[70] for Igor Pro employing a spherical micelle model.

Differential scanning calorimetry (DSC). Measurements were performed using a TA DSC25 Discovery series instrument using

aluminum Tzero pans/lids for PMMA samples, and Tzero pans and Tzero hermetic lids for diblock copolymer powders. Instrument calibration was performed using an indium standard. Purified $PLMA_{39}$-$PMMA_x$ (where x is 55 or 94) and $PLMA_{39}$-d_8PMMA_x (where x is 57 or 96) powders were obtained by precipitation of the corresponding 20% w/w diblock copolymer dispersion into a ten-fold excess of 2-propanol, followed by isolation via filtration and drying *in vacuo* for 24 h. For DSC analysis, each diblock copolymer was heated to 200 °C for 5 min, followed by cooling to 40 °C (allowing 5 min for thermal equilibration at this lower temperature). Subsequently, DSC measurements were performed on heating from 40 °C to 200 °C at a rate of 10 °C min^{-1}.

Results

Well-defined spherical diblock copolymer nanoparticles were prepared by a two-step PISA synthesis (**Scheme 1** and **Table 1**). First, a $PLMA_{39}$ precursor was prepared via RAFT solution polymerization of LMA in toluene at 70 °C (**Figure S1**, and **Equations S1** and **S2**). After purification, this precursor was chain-extended via RAFT dispersion polymerization of either deuterated or hydrogenous MMA at 20 % w/w solids in *n*-dodecane at 90 °C. At a certain critical PMMA DP, micellar nucleation occurred and the growing copolymer chains self-assembled to form spherical nanoparticles.

Proton NMR spectroscopy studies indicated high MMA conversions (>92%) for both PISA syntheses involving hydrogenous MMA (**Figure S2** and **Equation S3**). Similarly high conversions were obtained for the corresponding d_8PMMA

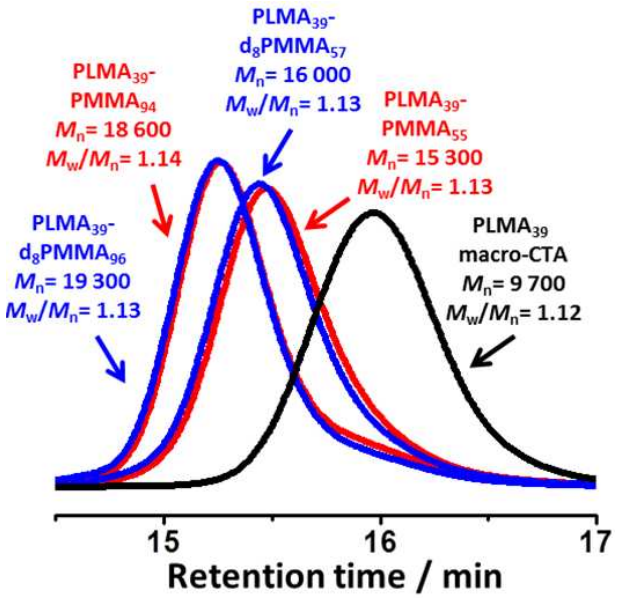

Figure 1. Normalized THF SEC traces recorded for $PLMA_{39}$ precursor block, $PLMA_{39}$-$PMMA_{55}$, $PLMA_{39}$-d_8PMMA_{57}, $PLMA_{39}$-$PMMA_{94}$ and $PLMA_{39}$-d_8PMMA_{96} using a refractive index detector (calibrated against a series of poly(methyl methacrylate) standards. These data indicate efficient chain extension in each case and almost identical molecular weight distributions for each pair of fully hydrogenous and core-deuterated diblock copolymers.

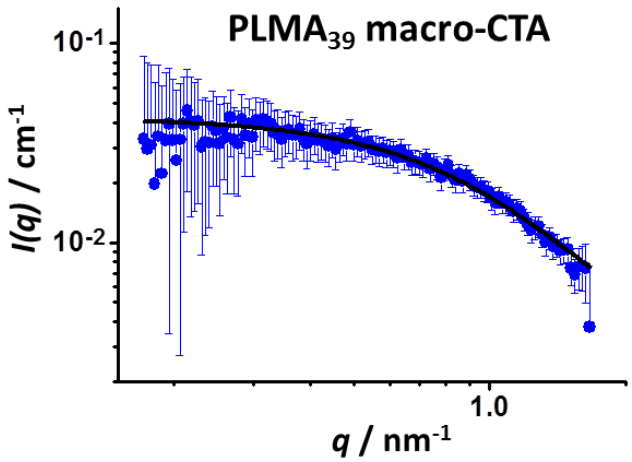

Figure 2. SAXS pattern recorded for a 1.0% w/w solution of the $PLMA_{39}$ precursor block dissolved in *n*-dodecane. The black line corresponds to the data fit obtained using the Debye function (**Equation S5**).[75] This analysis indicated a mean radius of gyration, R_g, of 1.91 ± 0.06 nm.

syntheses using deuterium NMR spectroscopy (**Figure S3** and **Equation S3**). THF SEC analysis of the four $PLMA_{39}$-$PMMA_{55}$, $PLMA_{39}$-$PMMA_{94}$, $PLMA_{39}$-d_8PMMA_{57} and $PLMA_{39}$-d_8PMMA_{96} diblock copolymers indicate efficient chain extension in each case, with a significant shift to lower retention times compared to the $PLMA_{39}$ precursor block (**Figure 1** and **Table 1**). Moreover, almost identical molecular weight distributions were obtained for the all-hydrogenous and corresponding core-deuterated copolymers, suggesting good reproducibility for these PISA syntheses when using MMA and d_8MMA.

SAXS was used to characterize the dimensions of the molecularly-dissolved $PLMA_{39}$ precursor (**Equation S5**) and the four types of diblock copolymer nanoparticles (**Equations S6-S14** in the Supporting Information). A 1.0% w/w solution of the $PLMA_{39}$ precursor in *n*-dodecane was analyzed in order to estimate the thickness of the corona block in the nanoparticles (**Figure 2**). The data were fitted using the Debye function[66] (**Equation S5**) which indicated a mean radius of gyration (R_g) of 1.91 ± 0.06 nm.

Hydrogenous $PLMA_{39}$-$PMMA_x$ and core-deuterated $PLMA_{39}$-d_8PMMA_x diblock copolymer dispersions were prepared at 20% w/w solids via PISA, and subsequently diluted with *n*-dodecane to 1.0 % w/w (0.7% v/v) dispersions prior to SAXS analysis (**Figure 3A, Tables S1** and **S2** in the Supporting Information). Each of the four scattering patterns recorded for the hydrogenous and core-deuterated nanoparticles exhibited a zero gradient at low *q*, which is consistent with the expected spherical morphology.[25] Satisfactory fits to these scattering curves were obtained when utilizing a spherical micelle model[67–69,71] (**Equations S6-S14**). SAXS patterns could be fitted on an absolute scale with no apparent nanoparticle core solvation at 20 °C (**Figure 3**). This was confirmed by variable temperature proton NMR experiments, which indicate that the nanoparticle cores only become appreciably solvated on heating above 80 °C (see **Figure S4**). A mean R_g value of around 2.00 ± 0.04 nm was determined for the $PLMA_{39}$ stabilizer chains

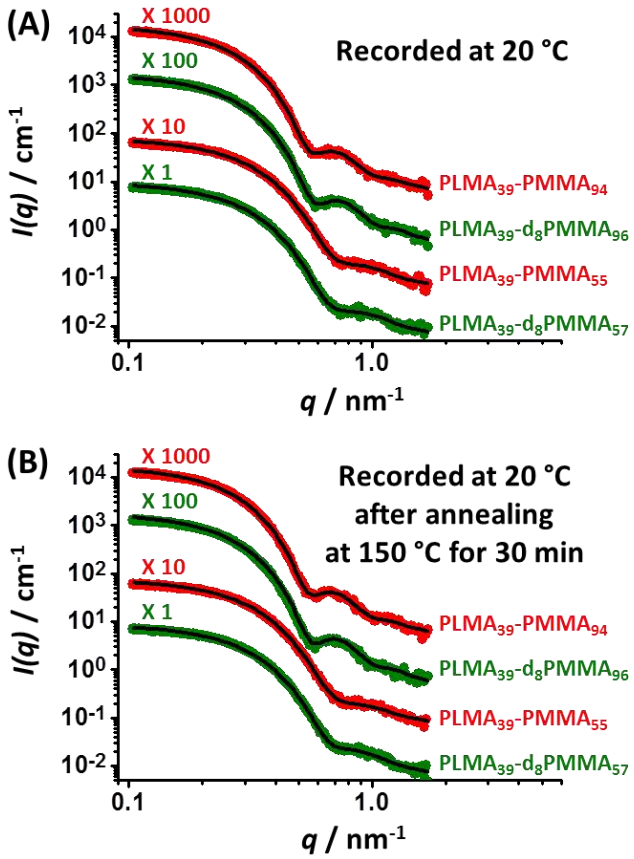

Figure 3. (A) SAXS patterns recorded at 20 °C for 1.0% w/w dispersions for each of the original four $PLMA_{39}$-$PMMA_x$ and $PLMA_{39}$-d_8PMMA_x diblock copolymer nanoparticles prepared via PISA (where x = 94 or 55 for $PMMA_x$ and 96 or 57 for d_8-$PMMA_x$). (B) SAXS patterns of the same four diblock copolymer nanoparticles recorded at 20 °C after annealing at 150 °C for 30 min. SAXS patterns are multiplied by arbitrary factors for the sake of clarity. The solid lines are best fits to the data obtained using a spherical micelle model (**Equations S6-S14**).[76–78,80]

at the surface of these nanoparticles, which is consistent with the R_g value of 1.91 ± 0.06 nm obtained by SAXS studies of the molecularly-dissolved $PLMA_{39}$ precursor (**Figure 2**). The small difference may originate from a slightly perturbed (stretched) chain conformation for the $PLMA_{39}$ stabilizer chains within the nanoparticles. Copolymer concentrations of around 0.5% v/v were obtained by SAXS analysis (**Table S2** in the Supporting Information), which are slightly lower than the expected value of 0.7% v/v. Nanoparticle core diameters of around 11 and 14 nm were determined for core-forming block DPs of 55 and 94, respectively. Total nanoparticle diameters (D) were calculated to be approximately 19 nm and 22 nm. The SAXS results indicated almost identical overall nanoparticle diameters when using either hydrogenous or deuterated MMA (**Table S3**).

These 1.0% w/w nanoparticle dispersions were then annealed to assess their thermal stability. Each dispersion was heated to 150 °C for 30 min. After returning to 20 °C, SAXS patterns of these annealed dispersions were very similar to those obtained for the original non-annealed dispersions. Fitting these SAXS

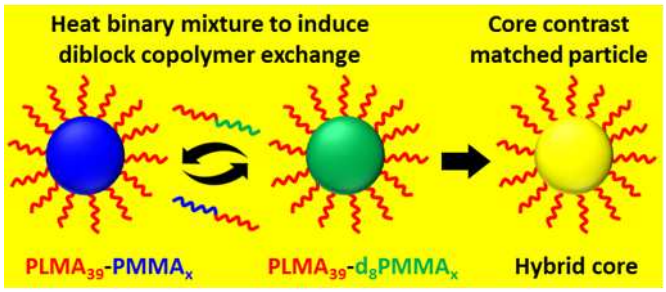

Scheme 2. Schematic representation of a time-resolved small-angle neutron scattering (TR-SANS) experiment in which copolymer chain exchange occurs between a binary mixture of spherical nanoparticles comprising hydrogenous and deuterated cores. As entropic mixing occurs, the neutron scattering intensity is reduced because the neutron SLD of the hybrid nanoparticle cores tends towards that of the binary solvent (which is a judicious mixture of 38% *n*-dodecane and 62% d_{26}-dodecane by volume).

patterns using the spherical micelle model produced comparable corona thicknesses and nanoparticle core diameters before and after annealing (see **Figure 3B**, and **Tables 1, S2** and **S3**). This suggests excellent colloidal and thermal stability for these nanoparticle dispersions under the stated conditions. Additionally, SAXS analysis confirmed that almost identical nanoparticles of two different sizes were obtained via RAFT-mediated PISA using either hydrogenous or deuterated MMA. The nanoparticle dimensions are not affected by heating such dispersions in turn up to 150 °C for 30 min. However, such SAXS experiments cannot be used to assess the extent of copolymer chain exchange that may occur between nanoparticles under these conditions. Instead, this aspect was examined using TR-SANS.

According to the literature,[39,40,61,41–48] TR-SANS can be used to examine whether copolymer chain exchange occurs between such nanoparticles. For a well-designed contrast variation experiment, neutron scattering can readily discriminate between the hydrogenous and deuterated core-forming blocks. Prior to TR-SANS analysis, a 1:1 v/v binary mixture of $PLMA_{39}$-$PMMA_x$ and $PLMA_{39}$-d_8PMMA_x nanoparticles was made up and subsequently diluted to 1.0 % w/w using a judicious blend of *n*-dodecane and d_{26}-dodecane, such that the final solvent mixture contained 38% *n*-dodecane by volume (**Equations S15, S16** and **Table S4** in the Supporting Information). This solvent composition was selected to ensure that its neutron SLD lies midway between those of the hydrogenous and deuterated PMMA cores. This binary mixture of nanoparticles was heated to various temperatures during the TR-SANS experiment to induce copolymer chain exchange. If copolymer chain exchange occurs between these two types of nanoparticles, then the SLD of the hybrid (mixed) nanoparticle cores should tend towards that of the binary solvent (**Scheme 2**). Thus, the neutron scattering intensity, $I(q)$, should be gradually reduced over time, since this parameter is approximately proportional to the square of the neutron SLD contrast for the $PMMA_x/d_8PMMA_x$ blocks within the nanoparticle cores ($\Delta\xi^2$).[72]

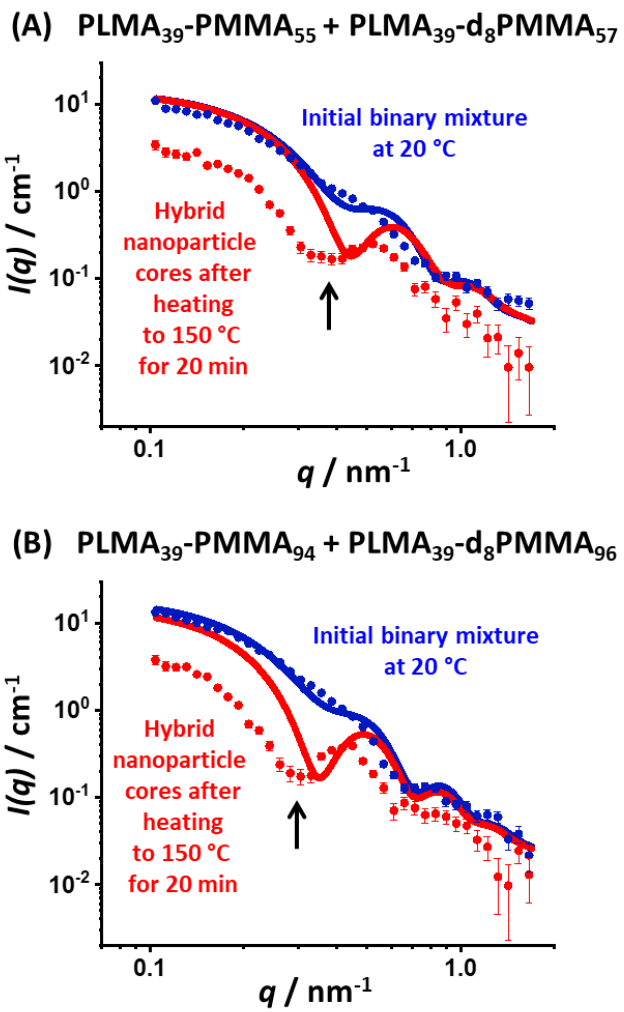

Figure 4. Experimental SANS patterns recorded for 1:1 binary mixtures by volume at 1.0% w/w solids of (A) $PLMA_{39}$-$PMMA_{55}$ and $PLMA_{39}$-d_8PMMA_{57} nanoparticles, and (B) $PLMA_{39}$-PMM_{94} and $PLMA_{39}$-d_8PMMA_{96} nanoparticles at 20 °C (blue data) and after 20 min at 150 °C (red data). In both cases, a pronounced minimum appears at intermediate *q* (see black arrows), which indicates that copolymer chain exchange occurs under these conditions. In each case, the solid red and blue curves correspond to predicted SANS patterns calculated from the respective SAXS models.

Unfortunately, it is non-trivial to fit the solvent-subtracted SANS scattering patterns recorded for the individual $PLMA_{39}$-$PMMA_x$ and $PLMA_{39}$-d_8PMMA_x nanoparticles using the model employed for SAXS analysis. This is because there is a non-linear relationship between scattering intensity and solvent composition for long-chain hydrocarbons.[73] Moreover, scattering from the hydrogenous lauryl side-chains of the PLMA stabilizer block becomes more pronounced in the SANS patterns owing to the additional contrast that is introduced by utilizing a binary solvent mixture. In contrast, the lauryl side-chains exhibit essentially the same SLD as the solvent used for SAXS analysis. Introduction of d_{26}-dodecane leads to additional contrast for SANS, so the bottle brush-like structure of the $PLMA_{39}$ stabilizer is highlighted by this technique but not by SAXS. This phenomenon particularly affects the scattering pattern at high *q*, which corresponds to relatively short length scales. Therefore, the SAXS data obtained for the $PLMA_{39}$-$PMMA_x$ and $PLMA_{39}$-d_8PMMA_x spherical nanoparticles (**Figure 3**) were used to predict the SANS scattering patterns expected for both the initial binary mixture of nanoparticles and the final hybrid (mixed) nanoparticles, where the latter species comprise nanoparticle cores that are contrast-matched to the solvent mixture. This was achieved by replacing the X-ray SLDs for each block and the binary solvent mixture with the corresponding calculated neutron SLDs (**Table S1**), while fixing all other model parameters. SANS patterns of the initial binary mixture were calculated for both the $PLMA_{39}$-$PMMA_{55}$ + $PLMA_{39}$-d_8PMMA_{57} nanoparticles and the $PLMA_{39}$-$PMMA_{94}$ + $PLMA_{39}$-d_8PMMA_{96} nanoparticles by assuming data additivity for each system as predicted from their respective SAXS models. SANS patterns for the hybrid (mixed) nanoparticles were calculated for each system assuming that the final micelle cores are composed of $PMMA_{55}$ and d_8PMMA_{57} in equivolume (1:1) proportions (**Figures 4A** and **4B**). In each case, literature values for the densities of PMMA and *n*-dodecane at 20 °C and 150 °C were used[63] to calculate the neutron SLD of each block at these temperatures (with the same temperature-dependence for the PMMA density being assumed for the PLMA and d_8PMMA blocks).

As expected, the predicted SANS scattering patterns for the final hybrid (mixed) nanoparticles exhibited a significant reduction in scattering intensity, with a pronounced minimum appearing at intermediate *q* in each case. Experimental SANS data confirmed these predictions: a progressive reduction in the overall neutron scattering intensity was observed over time (**Figures 4C** and **4D**). At the start of the experiment, the experimental scattering curves were similar to the predicted SANS patterns (compare the two pairs of blue and red curves shown in **Figures 4A** and **4B**). However, as copolymer chain exchange occurred, a distinct minimum was observed at intermediate *q* owing to the lack of contrast between the neutron SLD of the solvent mixture and that of the hybrid nanoparticle cores (see black arrows in **Figures 4**). The same approach was previously utilized by Lodge *et al.*[40–42,44–46,48,61] and Lund and co-workers[39,43,47,50–53,74] when investigating copolymer chain exchange between diblock copolymer micelles prepared using a traditional post-polymerization processing route (i.e. a solvent switch).

Both the experimental and predicted SANS data shown in **Figure 4** suggest that heating the initial binary mixture of $PLMA_{39}$-$PMMA_x$ and $PLMA_{39}$-d_8PMMA_x nanoparticles causes a reduction in the total neutron scattering intensity. This is because the neutron SLD of the isotopically heterogeneous nanoparticle cores tends to that of the binary solvent mixture as a result of entropically-driven copolymer chain exchange, which leads to the formation of hybrid (mixed) nanoparticle cores. However, some residual scattering is still observed owing to the hydrogenous nature of the $PLMA_{39}$ stabilizer block. The extent of copolymer exchange can be determined using the invariant scalar form of the total scattering (*Q*):

$$Q = \int_{q_{min}}^{q_{max}} I(q) \times q^2 \times dq \quad (2)$$

Q was calculated within the q_{min} and q_{max} limits defined by the q range used for the TR-SANS measurements. This parameter depends solely on the volume fraction of scattering components and their neutron SLD contrast and not on the nanoparticle morphology.[75] Thus Q is well-suited for monitoring the redistribution of copolymer chains to form hybrid (mixed) nanoparticle cores since this leads to a progressive reduction in neutron contrast, assuming that the SLD is constant across the mixed cores. This analytical approach differs from that reported in the literature, where changes in neutron scattering intensity at low angles [$R(t)$] were used to monitor the redistribution of copolymer chains.[40–43] However, nanoparticle core solvation by hot solvent (confirmed by variable temperature proton NMR spectroscopy studies on these dilute $PLMA_{39}$-$PMMA_x$ dispersions, see **Figure S4**) reduces the neutron scattering intensity significantly (see **Figure S5**). In principle, this means that it is difficult to compare neutron scattering intensities for nanoparticle dispersions over a broad temperature range. In view of this potential problem, we chose to use the scattering invariant, Q, which considers all data points to be equally important. This parameter is better suited for the present study because changes in the SANS patterns become more pronounced at intermediate q (see **Figure 4**). Nevertheless, broadly similar results were observed when using the more well-established $R(t)$ approach (see **Figure S6** and **Equation S18**). However, larger deviations in $R(t)$ were observed for the hybrid (mixed) nanoparticles at 150 °C. Thus it seems that both methods can be used to interpret the TR-SANS data but we focus on the scattering invariant approach in the present study.

The variation in Q during annealing at various temperatures is shown in **Figure 5**. Initially, each binary mixture of hydrogenous and core-deuterated nanoparticles was heated to 150 °C. These TR-SANS experiments revealed a striking difference between the 19 nm and 22 nm nanoparticles. For the smaller nanoparticles, fully mixed hybrid nanoparticle cores were formed within 3 min at this temperature, whereas the scattering intensity arising from the larger nanoparticles required 8 min at 150 °C to attain an approximately constant (lower) Q value. Both binary mixtures of nanoparticles exhibited faster copolymer exchange rates at higher temperatures. Moreover, the exchange rate for the shorter copolymer chains is significantly faster than that for the longer copolymer chains. These findings are consistent with observations made by Bates and co-workers for PEP-PS micelles, whereby a longer core-forming PS block led to significantly slower exchange kinetics.[40–42,44] Similar observations have been reported by Zinn *et al.* for diblock copolymer micelles in aqueous media.[43,47,51].

These data show that maximum core homogeneity owing to copolymer exchange is achieved more quickly at higher temperatures. Moreover, higher temperatures produce lower final Q values after 20 min. Since this invariant is a measure of homogeneity, this suggests that higher temperatures yield more homogeneous nanoparticle cores. This may indicate a higher proportion of molecularly-dissolved copolymer chains under such conditions, which would also cause a higher degree of core solvation. Variable temperature proton NMR

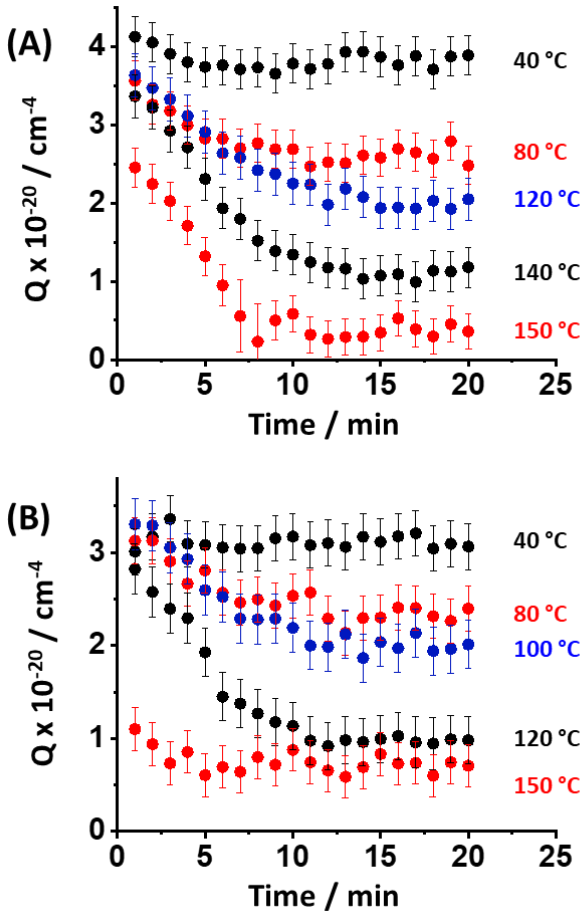

Figure 5. Heating binary mixtures of (A) $PLMA_{39}$-$PMMA_{94}$ and $PLMA_{39}$-d_8PMMA_{96} nanoparticles of around 22 nm diameter and (B) $PLMA_{39}$-$PMMA_{55}$ and $PLMA_{39}$-d_8PMMA_{57} nanoparticles of around 19 nm diameter causes a reduction in the scattering invariant *(Q)* during a TR-SANS experiment. The reduction in Q over time is the result of a reduction in neutron contrast for the nanoparticle cores owing to copolymer exchange. Higher temperatures result in faster rates of copolymer chain exchange between nanoparticles.

spectroscopy studies of the $PLMA_{39}$-$PMMA_{55}$ and $PLMA_{39}$-$PMMA_{94}$ dispersions were performed between 20 °C and 150 °C. The initial spectra recorded at 20 °C did not exhibit any discernible PMMA signals, indicating negligible nanoparticle core solvation under such conditions. However, PMMA signals gradually appeared at elevated temperatures, indicating increasing core solvation and/or a higher fraction of molecularly dissolved copolymer chains (**Figure S4**). Bearing in mind the inherent experimental error in these TR-SANS experiments, minimal change in Q was observed at 40 °C regardless of the nanoparticle diameter. This suggests that very slow (if any) copolymer exchange occurs at this temperature. This is understandable because these data were collected well below the T_g of the PMMA core-forming block, which is around 88 °C in the solid state (**Figure 6**). This is significantly lower than the T_g for a PMMA homopolymer of comparable DP. For example,

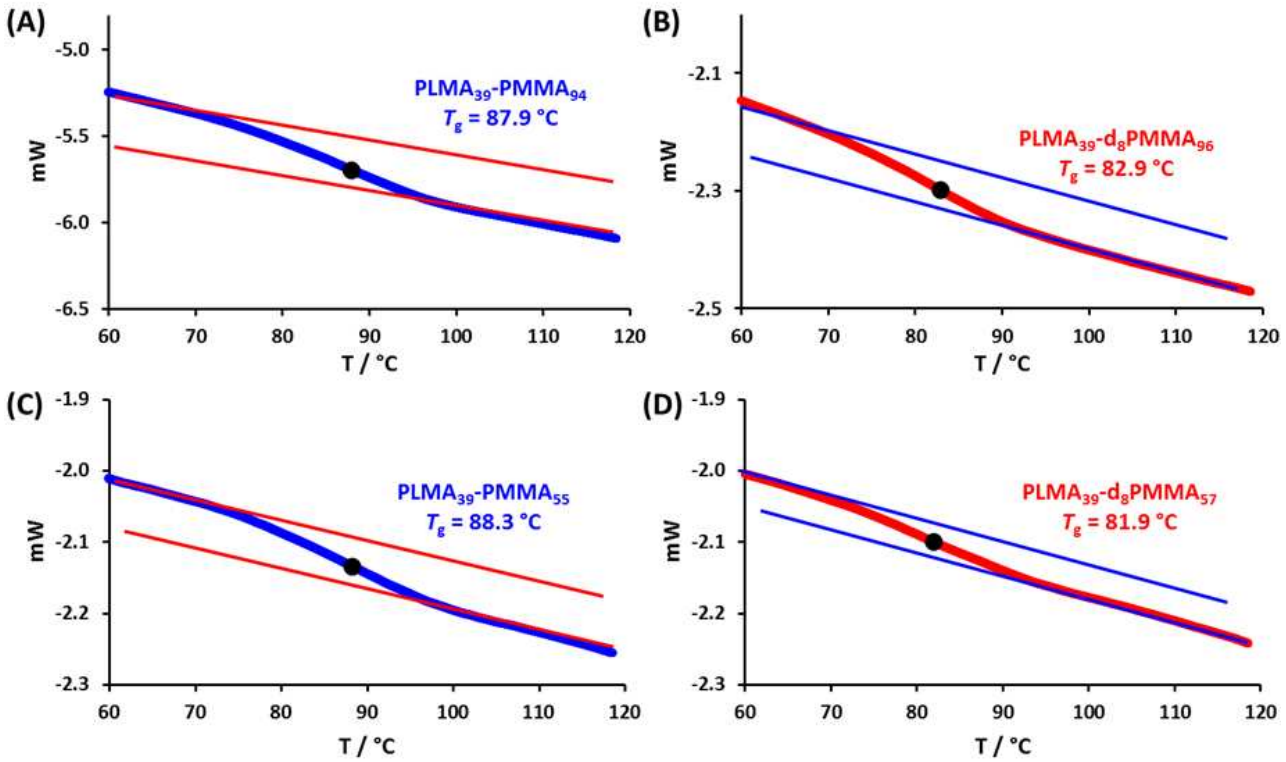

Figure 6. PMMA T_g determination via DSC for (A) $PLMA_{39}$-$PMMA_{94}$, (B) $PLMA_{39}$-d_8PMMA_{96}, (C) $PLMA_{39}$-$PMMA_{55}$ and (D) $PLMA_{39}$-d_8PMMA_{57}. Diblock copolymers were purified by precipitation of the 20% w/w nanoparticle dispersion into 2-propanol followed by filtration. T_g values for hydrogenous PMMA appear to be around 88 °C, while the semi-deuterated diblock copolymer exhibits a T_g of around 82 °C.

$PMMA_{102}$ has a T_g of around 120 °C (N.B. A T_g of approximately 127 °C was determined for PMMA homopolymers with DPs greater than 1270) (**Figure S7** in the Supporting Information). However, **Figure 5** indicates that copolymer chain exchange can certainly occur at 80 °C because a significant reduction in the scattering invariant was observed at this temperature.

Compared to the polystyrene-core micelles in non-polar media studied by the Minnesota team, copolymer chain exchange occurs on a relatively short time scale for these PMMA-core micelles.[40–42,44,46] However, the relatively low DPs of 57 and 94 for the core-forming blocks employed in the present study are expected to produce significantly lower T_g values compared to that for polystyrene (T_g. = 107 °C).[76] This important point is confirmed by DSC studies, which indicate T_g values for the hydrogenous and deuterated PMMA blocks of 82-88 °C, respectively (see **Figure 6** and **Table 1**). In this context, we also use DSC to illustrate how the T_g varies with PMMA DP for a series of well-defined PMMA homopolymers (see **Figure S7**). Thus, it is perhaps not surprising that copolymer exchange occurs much more quickly in the present study.

Discussion

All TR-SANS studies were performed using 1.0 % w/w nanoparticle dispersions. At such a low copolymer concentration, the micelle fusion/fission mechanism seems rather unlikely because there will be far fewer inter-particle collisions under such conditions. Moreover, both Lodge and co-workers[40–42,44–46,48,61] and the Lund group[43,47] show that the chain expulsion/insertion mechanism is consistent with the experimental observations. However, the nanoparticles examined in this study have somewhat lower core-forming block DPs and hence significantly lower T_g values; these two differences are the most likely explanation for the much faster copolymer exchange rates observed herein. Further research is clearly warranted to distinguish between the micelle fusion/fission and chain expulsion/insertion mechanisms. In this context, our recent studies[25,30] indicate a significant increase in aggregation number during a related RAFT PISA synthesis. This is best explained by fusion between well-solvated nascent nanoparticles during the early stages of this dispersion polymerization formulation. Moreover, a micelle fusion mechanism best explains the formation of the worm-like micelles that can be formed under certain conditions. Such highly anisotropic nanoparticles are unlikely to be formed solely via exchange of individual copolymer chains. However, in this case micelle fusion/fission is expected to be favored by (i) the much higher copolymer concentrations of 10-50% w/w typically employed for PISA syntheses and (ii) extensive solvation of the growing core-forming chains by the unreacted monomer, which effectively acts as a processing aid or co-solvent.

The TR-SANS data reported herein indicate that there is exchange of copolymer chains between $PLMA_{39}$-$PMMA_x$ spheres prepared via PISA at 90 °C, which is the reaction

temperature used for their synthesis. Based on the literature, it is reasonable to assume that this occurs via the chain expulsion/insertion mechanism. During PISA, the unreacted MMA monomer swells the nanoparticle cores, thus accelerating the rate of polymerization[21] while also acting as a vital processing aid (or co-solvent) for the insoluble growing PMMA chains by enhancing their mobility. Thus it is very likely that the same copolymer exchange mechanism also operates immediately after the micellar nucleation event during PISA, when the insoluble PMMA blocks are relatively short and the nascent nanoparticles are highly monomer-swollen. However, the energy penalty required to remove a copolymer chain from such nanoparticles becomes much greater for longer core-forming blocks. Thus the chain expulsion/insertion mechanism should become increasingly unlikely as the core-forming chains grow longer and the solvating MMA monomer gradually becomes depleted. Furthermore, PISA syntheses conducted at low copolymer concentrations using relatively long stabilizer blocks typically yield kinetically-trapped spheres.[25,28,35] For such formulations, there is likely to be a gradual transition from ergodic (dynamic) spherical micelles to non-ergodic (frozen) micelles during the polymerization, particularly when targeting relatively long core-forming blocks.

In contrast, the formation of highly anisotropic worms during PISA is believed to proceed via 1D fusion of multiple spheres, i.e. by a micelle fusion/fission mechanism.[35] This hypothesis is consistent with the observation that worms typically cannot be obtained at relatively low copolymer concentrations in PISA syntheses[33] because this mechanism becomes much less likely under such conditions. Moreover, worms are normally only obtained when targeting relatively short stabilizer blocks.[35] Again, this is understandable because weaker steric stabilization of the nascent spherical nanoparticles promotes their 1D fusion. Finally, the formation of worms (and vesicles) requires relatively long core-forming blocks to be targeted, for which the chain expulsion/insertion mechanism of single copolymer chains mechanism becomes much less likely.

According to Bates and co-workers [40–42,44–46,48,61] and Zinn *et al.*[43,47] the micelle fusion/fission mechanism is highly unlikely to be applicable to conventional diblock copolymer micelles (or nanoparticles). We agree with these findings but contend that the monomer-swollen nanoparticles that grow during PISA are much more likely to be able to undergo micelle fusion/fission than nanoparticles prepared via post-polymerization processing in the absence of any monomer (or other co-solvent). Thus, this mechanism appears to be the most likely explanation for the formation of highly anisotropic worms, during many PISA syntheses.[33,35] Indeed, 'segmented' worms comprising partially fused spheres can be observed by TEM for certain formulations.[77]

In summary, both the chain expulsion/insertion mechanism and micelle fusion/fission mechanism are likely to play important roles during PISA, with their relative prevalence depending on the precise formulation. Finally, we note that using thermal initiators with differing decomposition temperatures (or utilizing photo-initiation at ambient temperature) could substantially affect the rate of copolymer chain exchange during PISA, which may in turn influence the evolution in copolymer morphology.[78] Clearly, more research is warranted to examine the intriguing hypotheses outlined above.

Conclusions

Two pairs of hydrogenous $PLMA_{39}$-$PMMA_x$ and core-deuterated $PLMA_{39}$-d_8PMMA_x diblock copolymers (where x is 55 or 94 for the hydrogenated species, and 57 or 96 for the core-deuterated species) were synthesized in the form of sterically-stabilized nanoparticles via RAFT-mediated PISA in *n*-dodecane. NMR spectroscopy studies confirmed high monomer conversions were achieved in each case, and SEC analysis indicated almost identical narrow molecular weight distributions ($M_w/M_n \leq 1.14$) for each pair. Binary mixtures of hydrogenous and core-deuterated nanoparticles were analyzed by TR-SANS at various temperatures to examine whether any copolymer chain exchange occurs. This technique provides compelling evidence for entropic mixing of the copolymer chains, with the rapid formation of more weakly scattering nanoparticles comprising hybrid (mixed) cores at 80 °C or above. The rate of copolymer chain exchange is strongly temperature-dependent, with higher temperatures leading to faster exchange. Moreover, significantly faster chain exchange kinetics were observed for the shorter PMMA block (DP = 55) compared to the longer PMMA block (DP = 94).

These results are fully consistent with the TR-SANS studies reported by Lund *et al.* and Bates, Lodge and co-workers.[40,42,44] When considered in the context of RAFT-mediated PISA, this suggests that the chain expulsion/insertion mechanism is highly likely for monomer-swollen nascent micelles but should become much less important as the core-forming block DP increases (and also under monomer-starved conditions). However, a micelle fusion/fission mechanism remains the most logical explanation for the formation of worms from spheres during PISA, especially given that such anisotropic morphologies are typically not generated when performing PISA syntheses at relatively low copolymer concentration. It is perhaps worth emphasizing here that the latter mechanism should be favored by (i) the use of a relatively short stabilizer block[33] and (ii) the well-established monomer solvation of the growing core-forming blocks during PISA[21], which significantly increases their chain mobility.

Conflicts of interest

There are no conflicts to declare.

Acknowledgements

We acknowledge Dr Isabelle Grillo (Institut Laue-Langevin, ILL) for performing preliminary SANS measurements. Lubrizol is thanked for funding a PhD studentship for E.J.C. and for permission to publish this work. S.P.A. acknowledges an EPSRC Established Career Particle Technology Fellowship (EP/R003009).

References

1 M. Szwarc, *Nature*, 1956, **178**, 1168–1169.
2 M. Szwarc, M. Levy and R. Milkovich, *J. Am. Chem. Soc.*, 1956, **78**, 2656–2657.
3 Y. Mai and A. Eisenberg, *Chem. Soc. Rev.*, 2012, **41**, 5969–5985.
4 S.-H. Choi, F. S. Bates and T. P. Lodge, *J. Phys. Chem. B*, 2009, **113**, 13840–13848.
5 Y. Ma and T. P. Lodge, *Macromolecules*, 2016, **49**, 3639–3646.
6 G. Moad, E. Rizzardo and S. H. Thang, *Aust. J. Chem.*, 2012, **65**, 985–1076.
7 G. Moad, E. Rizzardo and S. H. Thang, *Aust. J. Chem.*, 2009, **62**, 1402–1472.
8 G. Moad, E. Rizzardo and S. H. Thang, *Acc. Chem. Res.*, 2008, **41**, 1133–1142.
9 G. Moad, E. Rizzardo and S. H. Thang, *Polymer (Guildf).*, 2008, **49**, 1079–1131.
10 E. Rizzardo, M. Chen, B. Chong, G. Moad, M. Skidmore and S. H. Thang, *Macromol. Symp.*, 2007, **248**, 104–116.
11 S. Perrier, *Macromolecules*, 2017, **50**, 7433–7447.
12 D. J. Keddie, *Chem. Soc. Rev.*, 2014, **43**, 496–505.
13 J. Tan, H. Sun, M. Yu, B. S. Sumerlin and L. Zhang, *ACS Macro Lett.*, 2015, **4**, 1249–1253.
14 M. H. Stenzel, *Chem. Commun.*, 2008, 3486–3503.
15 S. Pal, W. L. A. Brooks, D. J. Dobbins and B. S. Sumerlin, *Macromolecules*, 2016, **49**, 9396–9405.
16 P. De and B. S. Sumerlin, *Macromol. Chem. Phys.*, 2013, **214**, 272–279.
17 T. R. Barlow, J. C. Brendel and S. Perrier, *Macromolecules*, 2016, **49**, 6203–6212.
18 S. Perrier and P. Takolpuckdee, *J. Polym. Sci. Part A-Polymer Chem.*, 2005, **43**, 5347–5393.
19 O. J. Deane, J. R. Lovett, O. M. Musa, A. Fernyhough and S. P. Armes, *Macromolecules*, 2018, **51**, 7756–7766.
20 S. Sistach, M. Beija, V. Rahal, A. Brûlet, J.-D. Marty, M. Destarac and C. Mingotaud, *Chem. Mater.*, 2010, **22**, 3712–3724.
21 E. J. Cornel, S. Van Meurs, T. Smith, P. S. O'Hora and S. P. Armes, *J. Am. Chem. Soc.*, 2018, **140**, 12980–12988.
22 E. E. Brotherton, F. L. Hatton, A. A. Cockram, M. J. Derry, A. Czajka, E. J. Cornel, P. D. Topham, O. O. Mykhaylyk and S. P. Armes, *J. Am. Chem. Soc.*, 2019, **141**, 13664–13675.
23 S. L. Canning, G. N. Smith and S. P. Armes, *Macromolecules*, 2016, **49**, 1985–2001.
24 N. J. Warren, O. O. Mykhaylyk, D. Mahmood, A. J. Ryan and S. P. Armes, *J. Am. Chem. Soc.*, 2014, **136**, 1023–1033.
25 M. J. Derry, L. A. Fielding, N. J. Warren, C. J. Mable, A. J. Smith, O. O. Mykhaylyk and S. P. Armes, *Chem. Sci.*, 2016, **7**, 5078–5090.
26 M. J. Derry, L. A. Fielding and S. P. Armes, *Prog. Polym. Sci.*, 2016, **52**, 1–18.
27 J. Rieger, *Macromol. Rapid Commun.*, 2015, **36**, 1458–1471.
28 M. J. Derry, L. A. Fielding and S. P. Armes, *Polym. Chem.*, 2015, **6**, 3054–3062.
29 R. R. Gibson, S. P. Armes, O. M. Musa and A. Fernyhough, *Polym. Chem.*, 2019, **10**, 1312–1323.
30 E. R. Jones, O. O. Mykhaylyk, M. Semsarilar, M. Boerakker, P. Wyman and S. P. Armes, *Macromolecules*, 2016, **49**, 172–181.
31 Y. Pei, O. R. Sugita, L. Thurairajah and A. B. Lowe, *RSC Adv.*, 2015, **5**, 17636–17646.
32 Y. Pei, J.-M. Noy, P. J. Roth and A. B. Lowe, *J. Polym. Sci. Part A-Polymer Chem.*, 2015, **53**, 2326–2335.
33 L. A. Fielding, M. J. Derry, V. Ladmiral, J. Rosselgong, A. M. Rodrigues, L. P. D. Ratcliffe, S. Sugihara and S. P. Armes, *Chem. Sci.*, 2013, **4**, 2081–2087.
34 G. N. Smith, L. L. E. Mears, S. E. Rogers and S. P. Armes, *Chem. Sci.*, 2018, **9**, 922–934.
35 L. A. Fielding, J. A. Lane, M. J. Derry, O. O. Mykhaylyk and S. P. Armes, *J. Am. Chem. Soc.*, 2014, **136**, 5790–5798.
36 Y. Pei, L. Thurairajah, O. R. Sugita and A. B. Lowe, *Macromolecules*, 2015, **48**, 236–244.
37 Y. W. Pei, N. C. Dharsana, J. A. Van Hensbergen, R. P. Burford, P. J. Roth and A. B. Lowe, *Soft Matter*, 2014, **10**, 5787–5796.
38 B. Karagoz, C. Boyer and T. P. Davis, *Macromol. Rapid Commun.*, 2014, **35**, 417–421.
39 R. Lund, L. Willner, D. Richter and E. E. Dormidontova, *Macromolecules*, 2006, **39**, 4566–4575.
40 S. H. Choi, T. P. Lodge and F. S. Bates, *Phys. Rev. Lett.*, 2010, **104**, 47802.
41 S.-H. Choi, F. S. Bates and T. P. Lodge, *Macromolecules*, 2011, **44**, 3594–3604.
42 J. Lu, S. Choi, F. S. Bates and T. P. Lodge, *ACS Macro Lett.*, 2012, **1**, 982–985.
43 T. Zinn, L. Willner, V. Pipich, D. Richter and R. Lund, *ACS Macro Lett.*, 2015, **4**, 651–655.
44 J. Lu, F. S. Bates and T. P. Lodge, *ACS Macro Lett.*, 2013, **2**, 451–455.
45 J. Lu, F. S. Bates and T. P. Lodge, *Macromolecules*, 2015, **48**, 2667–2676.
46 J. Lu, F. S. Bates and T. P. Lodge, *Macromolecules*, 2016, **49**, 1405–1413.
47 T. Zinn, L. Willner, V. Pipich, D. Richter and R. Lund, *ACS Macro Lett.*, 2016, **5**, 884–888.
48 Y. Ma and T. P. Lodge, *Macromolecules*, 2016, **49**, 9542–9552.
49 E. Mueller, R. J. Alsop, A. Scotti, M. Bleuel, M. C. Rheinstadter, W. Richtering and T. Hoare, *Langmuir*, 2018, **34**, 1601–1612.
50 N. König, L. Willner, V. Pipich, T. Zinn and R. Lund, *Phys. Rev. Lett.*, 2019, **122**, 078001.
51 T. Zinn, L. Willner, R. Lund, V. Pipich and D. Richter, *Soft Matter*, 2012, **8**, 623–626.
52 R. Lund, L. Willner, V. Pipich, I. Grillo, P. Lindner, J. Colmenero and D. Richter, *Macromolecules*, 2011, **44**, 6145–6154.
53 R. Lund, L. Willner, J. Stellbrink, P. Lindner and D. Richter, *Phys. Rev. Lett.*, 2006, **96**, 068302.
54 L. Willner, A. Poppe, J. Allgaier, M. Monkenbusch and D. Richter, *Europhys. Lett.*, 2001, **55**, 667–673.

55 E. E. Dormidontova, *Macromolecules*, 1999, **32**, 7630–7644.
56 A. Halperin, *Macromolecules*, 2011, **44**, 5072–5074.
57 A. Halperin and S. Alexander, *Macromolecules*, 1989, **22**, 2403–2412.
58 T. Haliloğlu, I. Bahar, B. Erman and W. L. Mattice, *Macromolecules*, 1996, **29**, 4764–4771.
59 Y. Wang, C. M. Kausch, M. Chun, R. P. Quirk and W. L. Mattice, *Macromolecules*, 1995, **28**, 904–911.
60 D. J. Growney, O. O. Mykhaylyk and S. P. Armes, *Langmuir*, 2014, **30**, 6047–6056.
61 D. Zhao, Y. Ma and T. P. Lodge, *Macromolecules*, 2018, **51**, 2312–2320.
62 M. Semsarilar, V. Ladmiral, A. Blanazs and S. P. Armes, *Langmuir*, 2012, **28**, 914–922.
63 L. J. Fetters, D. J. Lohsey and H. Colby, *Physical Properties of Polymers Handbook*, Springer New York, 2nd edn., 2007.
64 P. E. Ngoepe, E. F. Lambson, G. A. Saunders and B. Bridge, *J. Mater. Sci.*, 1990, **25**, 4654–4657.
65 L. X. Fan, M. Degen, S. Bendle, N. Grupido and J. Ilavsky, *J. Phys. Conf. Ser.*, 2010, **247**, 12005.
66 P. Debye, *J. Phys. Colloid Chem.*, 1947, **51**, 18–32.
67 J. S. Pedersen and M. C. Gerstenberg, *Macromolecules*, 1996, **29**, 1363–1365.
68 J. S. Pedersen and P. Schurtenberger, *Macromolecules*, 1996, **29**, 7602–7612.
69 J. S. Pedersen, *J. Appl. Crystallogr.*, 2000, **33**, 637–640.
70 J. Ilavsky and P. R. Jemian, *J. Appl. Crystallogr.*, 2009, **42**, 347–353.
71 J. S. Pedersen and M. C. Gerstenberg, *Colloids Surfaces A Physicochem. Eng. Asp.*, 2003, **213**, 175–187.
72 I. Grillo, in *Soft Matter Characterization*, eds. R. Borsali and R. Pecora, Springer Netherlands, Dordrecht, 2008, pp. 723–782.
73 L. Arleth and J. S. Pedersen, *J. Appl. Crystallogr.*, 2000, **33**, 650–652.
74 R. Lund, L. Willner and D. Richter, in *Controlled Polymerization and Polymeric Structures: Flow Microreactor Polymerization, Micelles Kinetics, Polypeptide Ordering, Light Emitting Nanostructures*, eds. A. Abe, K. S. Lee, L. Leibler and S. Kobayashi, 2013, vol. 259, pp. 51–158.
75 R. J. Roe, in *Methods of X-ray and Neutron Scattering in Polymer Science*, ed. K. Binder, Oxford University Press, 1st edn., 2000.
76 J. Rieger, *J. Therm. Anal.*, 1996, **46**, 965–972.
77 P. Yang, L. P. D. Ratcliffe and S. P. Armes, *Macromolecules*, 2013, **46**, 8545–8556.
78 L. D. Blackman, K. E. B. Doncom, M. I. Gibson and R. K. O'Reilly, *Polym. Chem.*, 2017, **8**, 2860–2871.

